Stochastic Environmental Research and Risk Assessment
https://doi.org/10.1007/s00477-024-02783-3

ORIGINAL PAPER

Identifying regional hotspots of heatwaves, droughts, floods, and their co-occurrences

Marlon Vieira Passos[1,2] · Jung-Ching Kan[1,2] · Georgia Destouni[2,3] · Karina Barquet[1] · Zahra Kalantari[2,3]

Accepted: 16 July 2024

Abstract

In this paper we present a framework to aid in the selection of optimal environmental indicators for detecting and mapping extreme events and analyzing trends in heatwaves, meteorological and hydrological droughts, floods, and their compound occurrence. The framework uses temperature, precipitation, river discharge, and derived climate indices to characterize the spatial distribution of hazard intensity, frequency, duration, co-occurrence, and dependence. The relevant climate indices applied are Standardized Precipitation Index, Standardized Precipitation and Evapotranspiration Index (SPEI), Standardized Streamflow Index, heatwave indices based on fixed (HWI_S) and anomalous temperatures (HWI_E), and Daily Flood Index (DFI). We selected suitable environmental indicators and corresponding thresholds for each hazard based on estimated extreme event detection performance using receiver operating characteristics (ROC), area under curve (AUC), and accuracy, which is defined as the proportion of correct detections. We assessed compound hazard dependence using a Likelihood Multiplication Factor (LMF). We tested the framework for the case of Sweden, using daily data for the period 1922–2021. The ROC results showed that HWI_S, SPEI12 and DFI are suitable indices for representing heatwaves, droughts, and floods, respectively (AUC > 0.83). Application of these indices revealed increasing heatwave and flood occurrence in large areas of Sweden, but no significant change trend for droughts. Hotspots with LMF > 1, mostly concentrated in Northern Sweden from June to August, indicated that compound drought-heatwave and drought-flood events are positively correlated in those areas, which can exacerbate their impacts. The novel framework presented here adds to existing hydroclimatic hazard research by (1) using local data and historical records of extremes to validate indicator-based hazard hotspots, (2) evaluating compound hazards at regional scale, (3) being transferable and streamlined, (4) attaining satisfactory performance for indicator-based hazard detection as demonstrated by the ROC method, and (5) being generalizable to various hazard types.

Keywords Hydroclimatic hazard on land · Hazard mapping · Compound extreme land weather events · Index of land climate

Jung-Ching Kan, Georgia Destouni, Karina Barquet and Zahra Kalantari have contributed equally to this work.

✉ Marlon Vieira Passos
marlonvp@kth.se

Jung-Ching Kan
jungching.kan@sei.org

Georgia Destouni
georgia.destouni@natgeo.su.se

Karina Barquet
karina.barquet@sei.org

Zahra Kalantari
zahrak@kth.se

[1] Stockholm Environment Institute, Stockholm, Sweden

[2] Department of Sustainable Development, Environmental Science and Engineering (SEED), KTH Royal Institute of Technology, Stockholm, Sweden

[3] Department of Physical Geography, Stockholm University, Stockholm, Sweden

Published online: 30 July 2024

1 Introduction

Multi-hazard risk assessments have been developed to improve knowledge and management of complex climate risks towards a more integrated and holistic paradigm. Early mentions of multi-hazard research in Agenda 21 on sustainable development (UNCED 1993) contributed to the spread of this concept, which is now considered an essential element of disaster-risk management (Kappes et al. 2012). In this context, hydroclimatic hazards (heatwaves, droughts, floods) comprise a sub-category of natural hazards of particular interest due to their joint hydrological and atmospheric drivers and potentially devastating consequences for society. Hydroclimatic hazards may be increasing in magnitude and frequency due to climate change, with major impacts on the environment, human health, and infrastructure (Stevenson et al. 2022). Heatwaves have been linked to increased mortality rates in Europe (Stagliorio Coelho et al. 2023) and accelerated spread of infectious diseases such as Covid-19 (Lian et al. 2023). Droughts have direct negative impacts on agriculture, energy production, and water supply (Freire-González et al. 2017). Flooding can severely damage critical societal infrastructure, disrupting livelihoods, water and food storage, transportation, and energy supply networks (Intergovernmental Panel on Climate Change (IPCC) 2023). Co-occurrence of these hydroclimatic extremes can also intensify their potential impacts (Zscheischler et al. 2018). In Europe, more than 100 cities are particularly vulnerable to two or more types of adverse hydroclimatic effects (Guerreiro et al. 2018). Understanding the spatial-temporal and co-occurrence patterns of hydroclimatic hazards is critical for evaluating risks and selecting appropriate adaptation measures.

These patterns of hydroclimatic hazards can be identified using metrics derived from climate indices (Darand and Sohrabi 2018; Kirono et al. 2020; Serrano-Notivoli et al. 2022). Common metrics for droughts and wet periods include Standardized Precipitation Index (SPI) (Lloyd-Hughes and Saunders 2002), Standardized Precipitation and Evapotranspiration Index (SPEI) (Vicente-Serrano et al. 2010), and Standardized Streamflow Index (SSI) (Modarres 2007). To identify and quantify heatwave events, a Heatwave Intensity Index (HWI) has been proposed by the European Drought Observatory (Lavaysse et al. 2018). Using daily precipitation data, flood risks can be identified using Daily Flood Index (DFI), which has been applied in Australia, Fiji, and Bangladesh (Deo et al. 2015, 2019; Moishin et al. 2021).

Depending on the spatial resolution of the input data, climate indices can estimate hazard characteristics ranging from local to global scales. Although detection and experience of extreme weather events almost always occur and must be handled at local or regional level (Stone 2019), multi-hazard studies on droughts, heatwaves, and floods have typically been limited to global or continental scale, where spatial averaging to some degree masks extreme values (Thompson et al. 2023). Therefore, additional applied local-regional studies are needed for developing relevant adaptation and societal protection strategies. The shortcomings of large-scale approaches can be remedied to some extent through local observation data and locally validated models. Interpolation techniques can be employed to convert inputs into higher-resolution datasets that are more suitable for detecting extremes. The Kriging method has been widely applied to produce gridded time series from local observations of precipitation rates (Darand and Sohrabi 2018; Hu et al. 2016) and streamflows (Teutschbein 2024). Based on machine learning, the Gaussian Process Regression technique has been successfully applied to spatially interpolate air temperature (He et al. 2022) and daily precipitation (Kleiber et al. 2012).

Even though hydroclimatic indices may be able to quantify hazard risks at a variety of spatial scales, such indices have only been developed for and tested in relatively few locations so far and it is important to further test their suitability for applications in different geographical areas (Dikshit et al. 2021; Anshuka et al. 2019; Stenseth et al. 2003). Some studies have measured indicator performance through hit rate and false alarm ratios (Kumar et al. 2016) and best fitting models (Coscarelli et al. 2021). Uncertainty in climate change assessments is driven by a mismatch between climate models and actual observations, with input data quality playing a significant role (Kundzewicz et al. 2018). Input data quality uncertainties are minimized and hazard exposure can be more reliably mapped in terms of frequency, intensity, and duration through climate indices, tested and validated against actual, independently recorded and reported extreme events.

By assessing and validating different climate indices for distinct source of risks, a common framework can be established to reliably compare spatial and temporal variability of single hazard exposure, as well as potential compound effects of different hazards that may jointly lead to amplified impacts. Compound hazards have been typically classified as spatially compounding, temporally compounding, or preconditioned events (Zscheischler et al. 2020). To quantify spatially compounding hazards, i.e., co-occurring extremes at the same location, a likelihood multiplication factor (LMF) has been developed (Ridder et al. 2020).

The overall aim of this paper is to develop and test a data-driven and streamlined framework for identifying and mapping localized hotspots and analyzing trends in single and compound hydroclimatic hazards, thereby addressing

the need for region-specific multi-hazard assessments with locally available data and validated inputs. Novel contributions include this being the first known application of DFI for interpolated gridded datasets, as opposed to applications at specific observational sites, providing a spatial distribution of flood risks rather than just single-site risks. Additionally, we also present in this study a novel application of LMF at regional scale, and identify the best representative indicators for each type of hazard by use of the receiver operating characteristic (ROC) method (Rahmati et al. 2019) and by evaluating the hazard detection skill of different indicators against actual extreme events for a range of indicator value thresholds. The framework is developed and tested with the following specific objectives: (i) to comparatively investigate hydroclimatic indices for heatwaves, droughts, and floods based on available data for daily surface air temperature, precipitation, and river discharge; (ii) to test and validate the hazard detection ability of the different indices against historical records through the ROC method; (iii) to quantify the spatial distribution of single hazard intensity, duration, frequency, and change trends in terms of the identified respective optimal indicators; iv) to evaluate the spatial variability and seasonality of hazard co-occurrence at regional scale by estimating joint return periods, LMF, and change trends in these over time.

Application of the developed framework can contribute to reducing uncertainties of climate change and enhancing emergency preparedness for separate and joint impacts of heatwaves, droughts, and floods. The results of this study also test the hypothesis that the intensity, duration, and frequency of heatwaves, floods, and droughts are increasing due to climate change in the specific study area. Moreover, they test the hypothesis that these hydroclimatic extremes can produce compound effects with enhanced joint impact potential and important implications for disaster risk planning (Zscheischler et al. 2018).

The remainder of the paper is organized as follows. Section 2 presents the proposed framework, information regarding the study area, data collection, methodology to derive, validate and select hydroclimatic indices, and a procedure to evaluate single and co-occurring hazards. Section 3 presents the results, Sect. 4 discusses specific and general study implications and limitations, and Sect. 5 summarizes the main study findings and makes suggestions for future research.

2 Materials and methods

The framework developed consists of four main parts: (1) Data collection and processing; (2) validation and selection of indicators; (3) single hazard mapping; and (4) compound hazard mapping. Environmental indicators based on precipitation, temperature, and river discharge were compared against recorded extremes, to select suitable representations of heatwaves, floods, and droughts. Selected indicators were

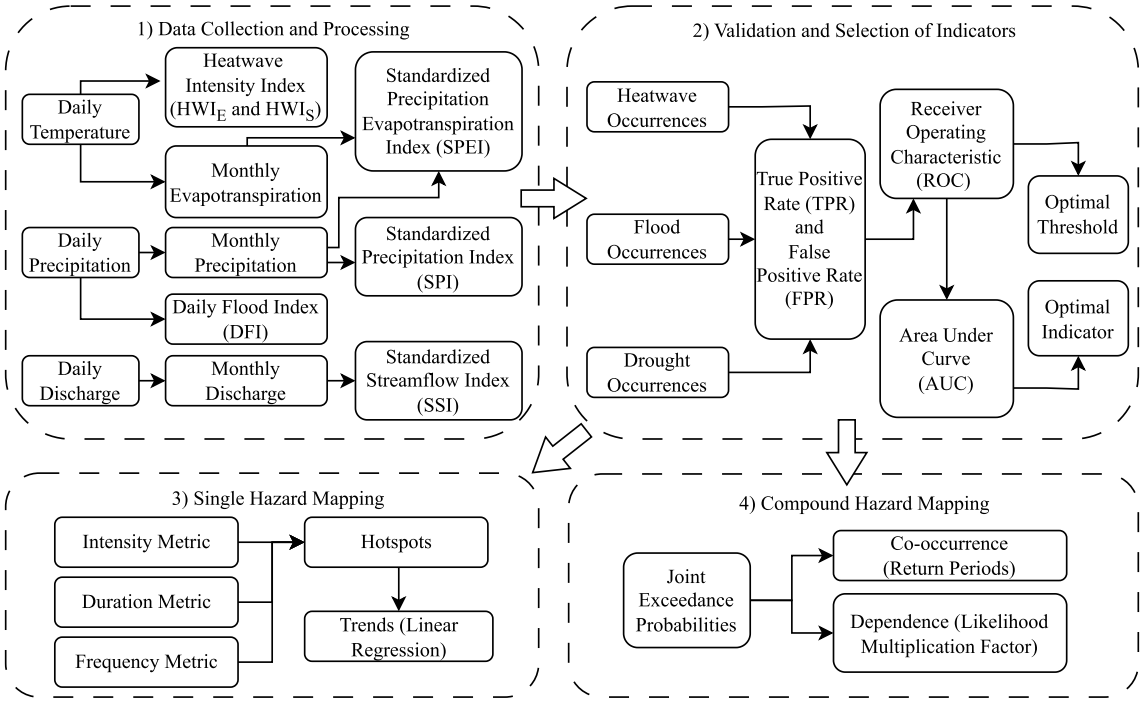

Fig. 1 Flowchart of the methodological study framework

used to map the spatial distribution of hotspots and trends of single and co-occurring extremes in the study region (Sweden). The methodology is depicted in Fig. 1.

2.1 Study area

The selected study area, Sweden, is located in Northern Europe (55–69 °N; 11–24 °E) and extends over three distinct climate zones according to the Köppen-Geiger climate classification (Beck et al. 2018). The southern region has a predominantly cold climate with warm summers, the central region and much of the northern region have a cold climate with cold summers, and part of the northern region has a polar climate (Fig. 2). Availability of hydrometeorological data from hundreds of weather stations in the last century makes Sweden a suitable case for investigating prolonged climate trends. The responsibility for implementing climate adaptation measures to maintain critical infrastructure services and disaster prevention is shared by the 291 municipalities in Sweden, highlighting the need for local-regional hazard mapping around the country (Englund and Barquet 2023).

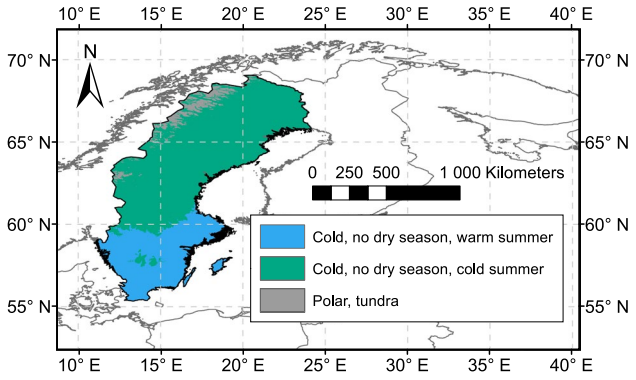

Fig. 2 The three main climate regions of Sweden

2.2 Data collection and processing

Data on all environmental parameters included in the analysis were retrieved from meteorological and hydrological observations available at the Open Data API (SMHI 2023b) provided by the Swedish Meteorological and Hydrological Institute (SMHI). To consider long-term hazard trends, the study period used was the 100-year period 1922–2021. We retrieved daily maximum and minimum air temperature data from 838 SMHI observation stations, daily precipitation data from 2038 meteorological stations, and modelled river discharge data from 448 locations. The river discharge data is provided by the national hydrological S-HYPE model system (Lindström et al. 2010), which is available at the VattenWeb database (SMHI 2024b). The hydrological model showed a deviation of ±10% for high flows and ±30% for low flows during the calibration period from 1999 to 2008 at 401 gauging stations (Bergstrand et al. 2014). The discrepancy between the number of gauging stations in the calibration reference and those in the dataset employed in this study is due to differences in model versions, with the most recent version as of March 2023 applied in this study. River discharge rates were normalized by catchment size for comparability, using 34149 sub-catchments with area above 1 km^2 provided by the SVAR database (SMHI 2024a). Figure 3 shows the locations of retrieved data points of temperature, precipitation, and river discharge. Daily temperature and 3-, 6- and 12-monthly accumulated precipitation datasets were spatially interpolated using Gaussian Process Regression techniques (Rasmussen and Williams 2005) to generate a gridded dataset (approximately 15 km × 15 km) with 100 latitude bands and 100 longitude bands for Sweden.

In addition to the directly observed and modelled meteorological and hydrological variables, we also considered related climate indices from the literature, due to their capability to characterize hydroclimatic hazards. Standardized indices were selected according to data availability, requiring precipitation, temperature, river discharge, geographical

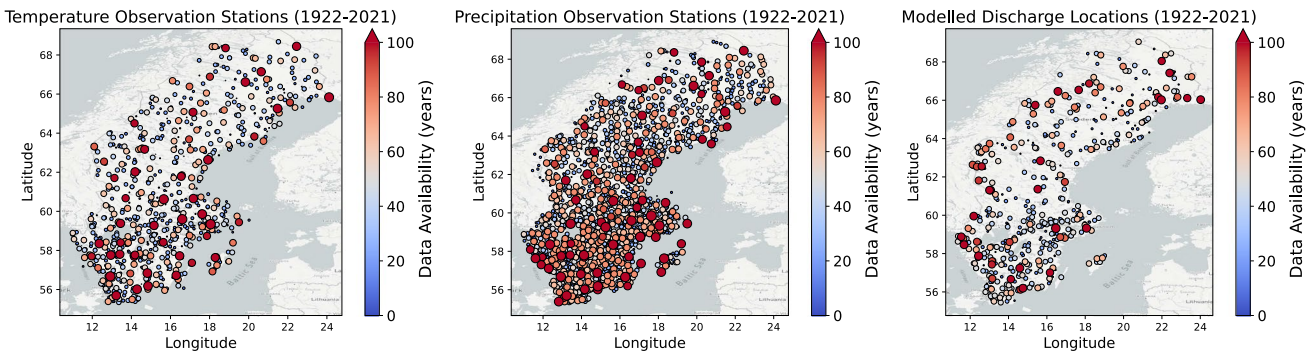

Fig. 3 Locations of meteorological and hydrological observations for Sweden obtained from SMHI Open Data API. Color and point size indicate data availability period

position, or a combination of these as inputs for practical implementation.

Heatwaves were investigated based on the Heatwave Index (HWI_E) proposed by the European Drought Observatory (EDO) (Lavaysse et al. 2018) and its modified version based on SMHI's definitions and thresholds for heatwaves (HWI_S). Daily HWI_E is calculated as the average of the differences between daily maximum and minimum temperatures and their corresponding thresholds. Hot days are defined by EDO as days when maximum T_x and minimum T_m temperatures are above calendar daily 90th percentiles Q and three consecutive hot days constitute a heatwave. HWI_E is then obtained at coordinates i and j at time t as

$$HWI_{E_{t,i,j}} = \frac{T_{x_{t,i,j}} - Q_{x_{t,i,j}} + T_{n_{t,i,j}} - Q_{n_{t,i,j}}}{2}. \quad (1)$$

According to SMHI's definition for Sweden, heatwaves occur when the maximum daily temperature is above 25 °C for five consecutive days (SMHI 2011). HWI_S is calculated as the difference between the maximum daily temperature and 25 °C, with positive values for hot days, expressed as

$$HWI_{S_{t,i,j}} = T_{x_{t,i,j}} - 25. \quad (2)$$

Adjusting the threshold allowed comparison of heatwave index performance based on absolute temperature, which may be more suitable for human health effects, against an index based on temperature anomalies, which is probably more suitable for assessing agricultural impacts (Lavaysse et al. 2018). Since heat-induced sensitivities vary significantly by region, it is recommended that absolute temperature thresholds are chosen according to local guidelines (Xiao et al. 2017; López-Bueno et al. 2021).

To quantify dry and wet season variability, we used Standardized Precipitation Index (SPI), Standardized Precipitation and Evapotranspiration Index (SPEI), and Standardized Streamflow Index (SSI). SPI and SPEI are commonly used indicators of meteorological droughts, while SSI is an indicator of hydrological droughts (Salimi et al. 2021). The standardized values of SPI, SPEI, and SSI typically vary from -2 (extreme drought) to 2 (extremely wet season). Since higher accumulated values of SPI, SPEI, and SSI indicate wetter conditions, these indices have been applied to monitor flood events. For instance, SPEI at 6- and 12-months accumulation periods with defined threshold 0.5 have been employed to evaluate wet events in the Yangtze River Basin (Yang et al. 2021), while SPI and SSI with threshold > 1 have been used to investigate the occurrence of floods in the Lake Chad in Africa (Nkiaka et al. 2017). We applied accumulation periods of 3, 6, and 12 months for these indices. SPI was calculated by fitting accumulated precipitation with gamma probability distributions and applying a transformation to convert cumulative probability distributions into the standard normal distribution (Lloyd-Hughes and Saunders 2002), obtained at month T as:

$$SPI_{T,i,j} = Y_{T,i,j} - \frac{C_0 + C_1 Y_{T,i,j} + C_2 Y_{T,i,j}^2}{1 + d_1 Y_{T,i,j} + d_2 Y_{T,i,j}^2 + d_2 Y_{T,i,j}^3}, \quad (3)$$

where:

$$Y_{T,i,j} = \sqrt{\ln[\frac{1}{(p_{AC_{T,i,j}})^2}}\ \text{for}\ p_{AC_{T,i,j}} \le 0.5, \quad (4)$$

$$Y_{T,i,j} = \sqrt{\ln \frac{1}{(1 - p_{AC_{T,i,j}})^2}}\ \text{for}\ p_{AC_{T,i,j}} > 0.5. \quad (5)$$

The following coefficient values are provided from the literature: $C_0 = 2.515517$, $C_1 = 0.802853$, $C_2 = 0.010328$, $d_1 = 1.432788$, $d_2 = 0.189269$, $d_3 = 0.001308$. The probability of exceeding a determined monthly accumulated precipitation p_{AC} was determined according to a gamma distribution. An analogous approach was applied to derive SSI, by employing monthly accumulated mean daily discharge rates instead of precipitation. (Modarres 2007). Potential evapotranspiration was calculated using the Hargreaves method (Hargreaves and Samani 1985) through temperature and extraterrestrial radiation based on the location's calendar day and latitude values. Monthly excess precipitation values were then employed to obtain SPEI (Vicente-Serrano et al. 2010), written as:

$$SPEI_{T,i,j} = W_{T,i,j} - \frac{C_0 + C_1 W_{T,i,j} + C_2 W_{T,i,j}^2}{1 + d_1 W_{T,i,j} + d_2 W_{T,i,j}^2 + d_2 W_{T,i,j}^3}, \quad (6)$$

where

$$W_{T,i,j} = \sqrt{-2 \ln(p_{EX_{T,i,j}})}\ \text{for}\ p_{EX_{T,i,j}} \le 0.5. \quad (7)$$

The probability of exceeding a determined monthly accumulated excess precipitation p_{EX} was estimated according to a log-logistic distribution. If $p_{EX_{T,i,j}} > 0.5$, the sign of the resultant $SPEI_{T,i,j}$ in Eq. 6 is inverted.

Daily Flood Index (DFI) is a metric designed to assess the occurrence of pluvial and fluvial floods on a daily basis, using historical rainfall data (Deo et al. 2015). The calculation involves two crucial factors: Effective Precipitation (P_E) and Available Water Resource Index (AWRI). P_E is determined by adding up the daily rainfall values for the preceding 365 days, adjusted by a time-based reduction function, written as:

$$P_{E_{t,i,j}} = \sum_{t=0}^{365} \left[\frac{\sum_{m=0}^{t} P_{m,i,j}}{t} \right]. \quad (8)$$

Where P is total daily precipitation. AWRI, indicating potential water availability, is derived by dividing P_E by a weighted factor (Byun and Lee 2002), described as

$$AWRI_{t,i,j} = \frac{P_{E_{t,i,j}}}{W_t}, \tag{9}$$

$$W_t = \sum_{t=1}^{365} \frac{1}{t}. \tag{10}$$

This weighting factor operates as an exponentially temporal reduction function spanning 365 days. DFI was computed at each location in this study as the difference between the day's P_E and the mean of the highest daily precipitation 1922–2021 ($P_{E_{i,j}^{\overline{\max}}}$), standardized by the standard deviation of the yearly maxima ($\sigma(P_{E_{i,j}^{\overline{\max}}})$):

$$DFI_{t,i,j} = \frac{P_{E_{t,i,j}} - P_{E_{i,j}}^{\overline{\max}}}{\sigma(P_{E_{i,j}}^{\overline{\max}})}. \tag{11}$$

While DFI can indicate flood danger, it does not estimate inundation areas or depth. More advanced techniques such as numerical modeling and detailed inputs would be required for this, which was outside of the scope of this study.

Table 1 shows the thresholds employed by each climate index to characterize extreme hydroclimatic conditions.

2.3 Environmental indicator performance and selection

Since the performance of environmental indicators in detecting extreme events varies for different regions, it is necessary to compare their ability to correctly represent these events. We compared the calculated climate indices and direct environmental parameters through the ROC method when selecting optimal indicators to be employed for mapping hazard hotspots and trends.

Lists of historical heatwave, drought, and flood events in Sweden were compiled from reports, articles, and fact sheets produced by SMHI and the Swedish Civil Contingencies Agency (MSB). The lists included type of hazard, municipality affected, and start and end date (Tables S1-S3 in Supplementary Material (SM)). In total, 10 heatwave, 10 drought, and 311 flood events were cataloged. Heatwave events were retrieved from a list of municipalities with longest number of hot days per year and longest continuous period with daily average temperatures of at least 22 °C, from 1961 to 2010 (SMHI 2011). Drought events comprised water shortage periods from 1930 s to 2010 s with significant negative impacts on agriculture, water supply and hydropower production (SMHI 2023a), without distinction between drought types or consistent criteria between events. Flood occurrences were retrieved from an extensive catalog of significant inundation events from 1924 to 2010. These events were due to various reasons, including excessive water levels in lakes, rivers and the sea, intense rainfall, snow melt, and stormwater system backflow (Alfredsson 2012). Indicator values of extreme event durations were retrieved at the nearest available location. Data on SSI, daily discharge, and precipitation were extracted from the nearest available source point. All other indicators were extracted from the interpolated grid dataset. For monthly datasets, the data were extracted at the nearest available time to the event (either before or after). Since droughts are longer events with imprecise documentation on beginnings and ends, this approximation does not significantly affect the detection performance evaluation. To represent normal conditions, indicator data were extracted for 10 random consecutive days over the 100-year study period in each Swedish municipality. The criteria for normal conditions were maximum daily temperature below 25 °C and average SPI12 values between − 0.5 and 0.5. Having a control group under non-hazard conditions was employed to improve the performance evaluation method. Applying the established criteria was useful for data rebalancing (Xue and Hall 2015), since, in reality, the number of days without hazards far exceeds the number of days when extremes occur.

Indicator performance was assessed using the selected evaluation metrics by comparing the hazard detection ability of the extracted indicator values at multiple thresholds against documented historical hazards. Hazards were detected whenever a particular indicator triggered the tested threshold. Indicators were tested against extracted data during their target hazard conditions and normal or non-hazard conditions, to ensure balanced data representation and more comprehensive testing results. Table 2 lists the minimum and

Table 1 Standard thresholds for quantifying heatwaves, droughts and floods according to different climate indices

Climate Index	Threshold	Description
DFI	> 0	Increased risk of flooding
HWI_E, HWI_S	> 0	Hot days, consecutive hot days indicates heatwaves (3 per EDO and 5 per SMHI)
	− 1.0 to − 1.5	Moderate drought conditions
	− 1.5 to − 2	Severe drought conditions
	< −2	Extreme drought conditions
	1.0 to 1.5	Moderate wet conditions
	1.5 to 2	Severe wet conditions
SPEI, SPI, SSI	> 2	Extreme wet conditions

HWI_E, European Drought Observatory Heatwave Index; HWI_S, SMHI Heatwave Index; SPI, Standardized Precipitation Index; SPEI, Standardized Precipitation and Evapotranspiration Index; SSI, Standardized Streamflow Index

Table 2 Indicators and corresponding threshold range for evaluation of hazard detection skill

Environmental Indicator	Threshold (minimum)	Threshold (maximum)	Interval	Hazard
3-Month Precipitation (mm)	0	500	20	Drought/Flood
6-Month Precipitation (mm)	0	800	20	Drought/Flood
12-Month Precipitation (mm)	0	1500	100	Drought/Flood
Normalized Daily Discharge (mm/day)	0	13518*	Variable	Flood
Daily Precipitation (mm)	0	200	Variable	Flood
DFI	− 4	4	0.5	Flood
HWI_E/ HWI_S (°C)	− 25	10	1	Heatwave
Max. Daily Temperature (°C)	1	41	2	Heatwave
Min. Daily Temperature (°C)	− 11	31	2	Heatwave
SPI/SPEI/SSI	− 3.5	3.5	0.5	Drought/Flood

*This high value corresponds to an extreme discharge rate of 2026 m^3/s occurring in May of 1984 when several municipalities were flooded along the Tornionjoki River in the county of Norrbotten, near the border between Sweden and Finland. While the corresponding yearly average river flow is approximately 400 m^3/s, the seasonal average discharge rate is much higher during spring thaw with severe ice breaks and even much higher discharge rates than that are plausible in combined events of both extreme precipitation and extreme snow and ice melt

maximum threshold values tested and intervals for each indicator and their corresponding hazards for detection. Intervals indicate the range of the tested thresholds, from minimum to maximum values. Threshold ranges and intervals were chosen to account for the entire distribution of the extracted data and yield complete ROC curves. Daily precipitation and discharge thresholds have variable intervals, so their entire sample distribution was tested more effectively through smoother ROC curves, since the distribution of those two variables skews towards smaller values due to the nature of catchment sizes and higher precipitation rates being significantly less frequent. The variable threshold intervals were then determined by selecting eleven values corresponding to equally spaced percentiles from zero to 100. Daily precipitation and normalized discharge rates were only applied to detect flood events with shorter duration, whereas accumulated precipitation rates were tested for detecting droughts. The way in which a hazard is detected depends on whether its corresponding threshold is of lower-bound or upper-bound type. Lower-bound thresholds indicate presence of hazards once the threshold value is exceeded, whereas upper-bound thresholds detect hazards when the indicator value falls below the threshold value. In this study, upper-bound thresholds were used to detect droughts and lower-bound thresholds to detect heatwaves and floods. For example, if the observed SPI in a given month was less than or equal to the adopted upper-bound threshold of -1, drought was detected in that particular month.

Indicator performance is generally evaluated in terms of true and false positive rates. True positives occur when predicted hazards agree with documented actual hazards, while false positives occur when the hazard is wrongly detected by the indicator. The true positive rate represents the proportion of correctly identified hazards out of all actual hazards, while the false positive rate is the fraction of incorrect hazard identifications among instances where no hazard is present. The optimal threshold maximizes accuracy, which is the ratio between correct observations over the total observations, defined as:

$$A_c = \frac{TP + TN}{TP + TN + FP + FN}, \tag{12}$$

where TP, TN, FP, and FN are the number of true positives, true negatives, false positives, and false negatives, respectively. Using true positive rates (TPR) and false positive rates (FPR), ROC curves can be created to illustrate the hazard detection skill of indicators under varied thresholds (Bradley 1997). The area under the curve (AUC) represents the overall ability of each indicator to discriminate between hazard conditions and normal conditions (Rahmati et al. 2019). In the context of hazard detection, a higher AUC value implies that an indicator has a higher likelihood of correctly classifying hazards and non-hazards, which is a sign of its effectiveness in identifying the target conditions. An ideal indicator achieves an AUC score of 1, while an AUC score close to 0.5 suggests that indicator performance is no more effective than random chance (Guvenir and Kurtcephe 2013). The ROC method has been applied in previous climate studies for evaluation of hydrological streamflow, flood and drought forecasts (Avand et al. 2021; He et al. 2018; Shin et al. 2020; Šípek and Daňhelka 2015).

2.4 Mapping single and compound hazards

Mapping of heatwave, drought, and flood hotspots was performed for single and compound hazards using the selected

indicators and thresholds to detect the start and end of the extreme events. First, spatial distributions of single hazard intensity, frequency, and duration were identified. Hazard duration was defined as the consecutive time period when the indicator threshold is exceeded. Hazard intensity was defined as the total sum of indicator values during the hazard duration, with daily frequency for heatwaves and floods and monthly frequency for droughts. Cumulative values over a decade were employed at each grid cell to describe historically critical areas. Projected changes in statistically significant areas were estimated through Mann–Kendall testing of accumulated values over time. Trends were considered only for statistically significant areas where the null hypothesis of no effect or relationship was rejected ($p = 0.05$).

Compound hazards were defined as the co-occurrence of various hydroclimatic drivers and/or hazards within a particular geographical area (Zscheischler et al. 2020). For analysis of co-occurrence of all three possible hazard pairs, joint return periods were estimated as the inverse of the joint occurrence probability for each grid cell (Ridder et al. 2020). To consider seasonal hazard variability, the analysis was conducted for each month of the year across the study period. Binary arrays X and Y were generated at every grid cell for each month of the year, to represent days when two distinct hazards occurred. A value of *1* was assigned for days when the indicator triggered a hazard, and *0* otherwise. A joint array Z to represent the intersection between the hazard pair was created as:

$$Z_i = \begin{cases} 1, & X_i = 1 \cap Y_i = 1 \\ 0, & \text{otherwise} \end{cases}. \tag{13}$$

The joint probability $P(X \cap Y)$ for a particular month of the year was calculated as the ratio between the sum of days where both hazards in a pair occurred simultaneously and the total number of days in the study period:

$$P(X \cap Y) = \frac{\sum_t Z^*(t,\ lat,\ lon)}{n_{days}} = \frac{W}{n_{days}}, \tag{14}$$

where W is the number of joint occurrences. The joint return period was then computed at each grid cell as the inverse of the joint probability and converted from days to years by dividing by the average number of days per month:

$$R_P(X \cap Y) = \frac{1}{P(X \cap Y) \times (\frac{365}{12})}. \tag{15}$$

To evaluate the spatial distribution of the dependence between hazard pairs, LMF was used (Zscheischler and Seneviratne 2017). This factor quantifies how co-occurring hazards are correlated, to investigate whether the occurrence of one hazard affects the likelihood of the other hazard happening, which could exacerbate their compound impacts. LMF was computed at each grid cell as the ratio between the observed probability of joint occurrence P_{actual} and the probability P_{indep} assuming complete independence between the hazards in each pair:

$$P_{actual} = \frac{\sum_t Z(t,\ lat,\ lon)}{n_{days}}, \tag{16}$$

$$P_{indep} = \frac{\sum_t X(t,\ lat,\ lon)}{n_{days}} \times \frac{\sum_t Y(t,\ lat,\ lon)}{n_{days}}. \tag{17}$$

Positive correlation between hazards is found for LMF values above 1, while LMF = 1 implies independent hazards, and negative LMF values indicate a negative correlation between the hazards in each pair. Statistical significance of joint exceedance of paired hazard values was tested at 5% level by employing a bootstrapping technique, which involves comparing 1000 resampled and actual time series (Ridder et al. 2020). This technique involves generating a resampled time series Y^* and then recalculating joint arrays Z^* with observed array X through equation 13 1000 times. Each time, the number of resampled realizations W^* is calculated as

$$W^* = \sum_t Z(t,\ lat,\ lon) + N, \tag{18}$$

where N is a noise array of random elements ranging from −0.0009 to 0.0009. The null hypothesis that joint exceedance by hazard X and hazard Y is introduced by random chance and does not involve any physical correlation between these hazards was rejected if the number of resampled realizations was higher than the number of observed realizations less than 5% of the time.

3 Results

3.1 Evaluation of hazard detection skill

Figure 4 shows the ROC curves used to assess the performance of the various indicators in detecting specific hazards for the whole of Sweden. For heatwave detection, the indicators HWI_E, HWI_S, and maximum and minimum daily temperature exhibited excellent discriminatory power, with AUC values approximately equal to the ideal score. These indicators achieved very high TPR at optimal thresholds (97–100%), while maintaining FPR below 0.8% at optimal thresholds. A minimum air temperature of 15 °C or higher was strongly associated with heatwave occurrence. Such strong performance is expected for heatwave detection, since both the adopted definition of the hazard and all indicators are based directly on air temperature data. HWI_S with

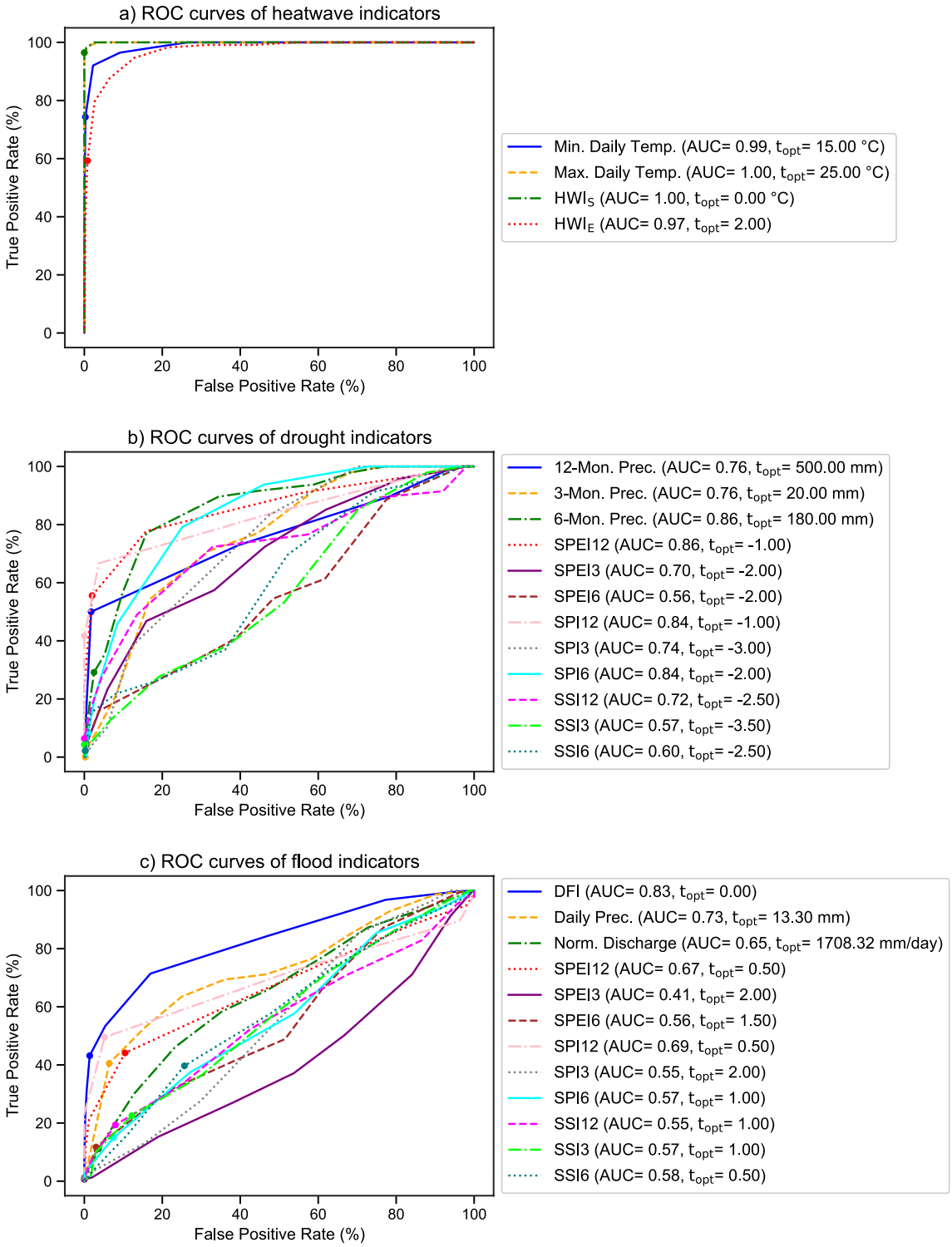

Fig. 4 Receiver operating characteristic (ROC) curves, area under the curve (AUC), and optimal thresholds (dots) of heatwave (**a**), drought (**b**), and flood (**c**) indicators. Optimal thresholds and area under curve are indicated as t_{opt} and AUC, respectively

$AUC = 1.00$ and positive values was selected here as the best indicator for detecting and describing heatwaves in Sweden.

The indicators for drought detection also demonstrate good performance (average AUC = 0.73), indicating strong discriminatory ability. Optimal thresholds corresponding to maximum accuracy for tested drought indices were all negative, consistent with the standard thresholds from the literature. Detecting historical droughts can be challenging

due to the subjectivity inherent in their definition and the simultaneous influence of multiple factors, including precipitation, river discharge, groundwater level, and soil moisture. Drought indices with higher accumulation periods (12 months) showed slightly stronger performance. SPEI12 ≤ -1 was selected to evaluate droughts in Sweden, due to its combination of high AUC and TPR (0.86 and 55%, respectively). This threshold corresponds to moderate to severe drought periods (Vicente-Serrano et al. 2010).

Flood detection was more challenging than detection of droughts and heatwaves. Some indicators, such as DFI and daily precipitation rates, performed reasonably well, with AUC values above 0.70, whereas others such as SPEI, SPI, and SSI show lower AUC values, suggesting limited discriminatory ability. These results suggest that, even though monthly standardized indicators can specify wet seasons, daily frequency indicators are required to detect flood events with reasonable accuracy. DFI with AUC = 0.83 was chosen here as the indicator to characterize floods in Sweden, with positive values representing increased danger.

Overall, the results indicate that the selected heatwave indicators are highly effective in hazard detection, the drought indicators are moderately effective, and the flood indicators vary in their effectiveness, with some more successful than others in discriminating between true positives and false positives.

3.2 Hotspots and trends in hydroclimatic hazards

3.2.1 Heatwaves

Heatwave mapping performed using the intensity index based on the SMHI definition ($HWI_S > 0$ °C) showed areas with 90th percentile decadal cumulative heatwave intensity and duration during the study period, and areas with the highest occurrence of heatwaves (Fig. 5). The 90th percentile

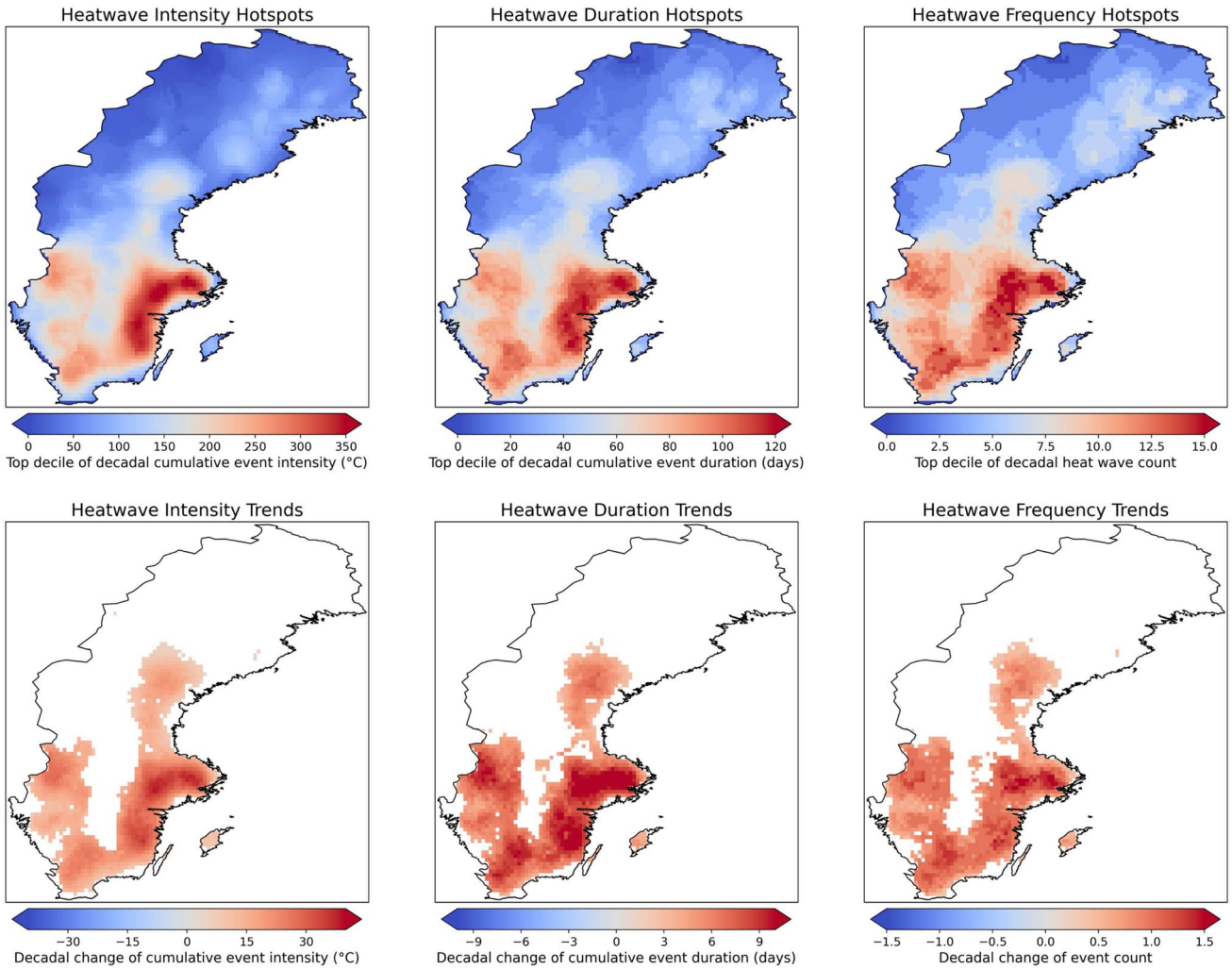

Fig. 5 Hotspots and trends in heatwave intensity, duration, and frequency in Sweden (SMHI heatwave Index, HWI_S)

cumulative decadal heatwave duration was up to 131 days in southeast Sweden. The highest heatwave intensity in the 100-year study period was observed in July 2018 in Kalmar County, in the south-east of Sweden. The most intense heatwave was also the longest observed, lasting 31 days in total. The total number of heatwaves detected in Sweden in the study period ranged from less than five near Kiruna in the far north to 111 in Södermanland County in the south-east. Heatwaves were found to be relatively less intense in coastal areas than inland areas, which can be attributed to cooling effects of coastal upwelling in the Baltic Sea (Suursaar 2020). Frequency analysis showed that heatwaves can be expected to occur on average at least once per year in most of Sweden, mainly in the period from June to August, but that occurrences are also possible in May, August, and September, especially in southern Sweden.

The yearly maxima of daily HWI_S were spatially averaged across grid points in Sweden to describe long-term trends (Figure S1 in SM). The spatially averaged intensity of heatwaves steadily increased from the beginning of the time series, reaching its highest value in 2018. Decadal increase or decrease trends investigated using Pearson's correlation coefficient at every grid point indicated increasing heatwave intensities in heavily populated areas in southern and eastern Sweden. Increasing trends in heatwave frequency and duration were also found for large areas in the south of the country. If these trends persist, heatwaves in critical southern areas may become one day longer and contain two more hot days per year on average by 2032.

3.2.2 Droughts

Drought hotspots and trends in Sweden were examined using SPEI12 with threshold ≤ -1. The spatially averaged SPEI12 values (Figure S2 in SM) revealed occurrence of extreme or severe droughts during the periods 1933–1934, 1947–1948, 1959–1960, 1976, 2003, and 2018–2019, which is consistent with historical records (SMHI 2023a). The driest month overall in Sweden was October 1947, which corroborates records showing that this year had one of the lowest annual average precipitation rates ever experienced, with major water shortages in many parts of Sweden (SMHI 2019). Over the long term, there was a consistent upward trend in the occurrence of wet seasons, which can be attributed to an overall increase in precipitation rates. This precipitation trend co-occurs with a temperature increase trend of climate warming, expected also to increase evapotranspiration rates.

Drought hotspots and trends from SPEI12 results are shown in Fig. 6. The most robust correlations between drought intensity, duration, frequency, and the emergence of prominent patterns were observed when these metrics were aggregated over a span of one decade. For consistent map visualization, drought intensities were inverted to yield absolute values. Drought duration at the decadal cumulative 90th percentile was longest in Halland County, located on the south-west coast of Sweden, reaching 86 months in the decade 1933–1942. This region also experienced the highest frequency of droughts, with dry months observed 22% of the time. Although the northernmost Swedish counties showed a relatively high frequency of droughts, this did not coincide with increased drought intensity or longer duration in those northern areas.

When droughts were catalogued and ranked according to their total intensity, the most intense drought event observed in the study period occurred in Norrbotten County, covering the most northern part of Sweden, between 1945 and 1948, with a total absolute SPEI12 intensity of 65.5 lasting 35 consecutive months. Most of the severe drought events in Sweden occurred before the 1960s, with only a few events occurring since 2000. Nevertheless, notable drought events were also identified in recent times, including some extended drought periods in Södermanland County, located just south of the capital Stockholm on the central to south-eastern coast of Sweden, from August 2016 to January 2018 and from September 2018 to November 2019. Over most of the country, no statistically significant drought trends were identified at 5% significance level using the Mann–Kendall method, with the exception of some areas in the west showing decreasing trends and a few locations in the southeast indicating some small localities with increasing frequency trends.

3.2.3 Floods

Mapping of flood hazard hotspots and trends produced for positive DFI values (Fig. 7) showed a widespread distribution of localized areas with higher flooding risks (Figure S3 in SM). Spatial correlation was observed between decadal cumulative flood hazard metrics, with an average correlation coefficient of 0.95 between intensity and duration, and 0.45 between intensity and frequency. At 90th percentile level, up to 38 flood-prone periods were observed at hotspots in a decade, while decadal cumulative flood hazard conditions in some areas reached up to 428 days. In periods identified as having the highest flood intensities, flood conditions sometimes persisted continuously for over 100 consecutive days. Historical records confirmed that the majority of these periods resulted in actual flooding events. Analysis of monthly patterns during the study period revealed a significant surge in the occurrence of flood conditions in July, reaching a peak in September, and gradually subsiding but remaining at elevated levels until the end of January.

The average number of days per year with flood conditions in Sweden increased during the study period, from on average 2.14 days in 1922–1971 to 5.35 days in 1972–2021. A further increase to an average of 8.11 days

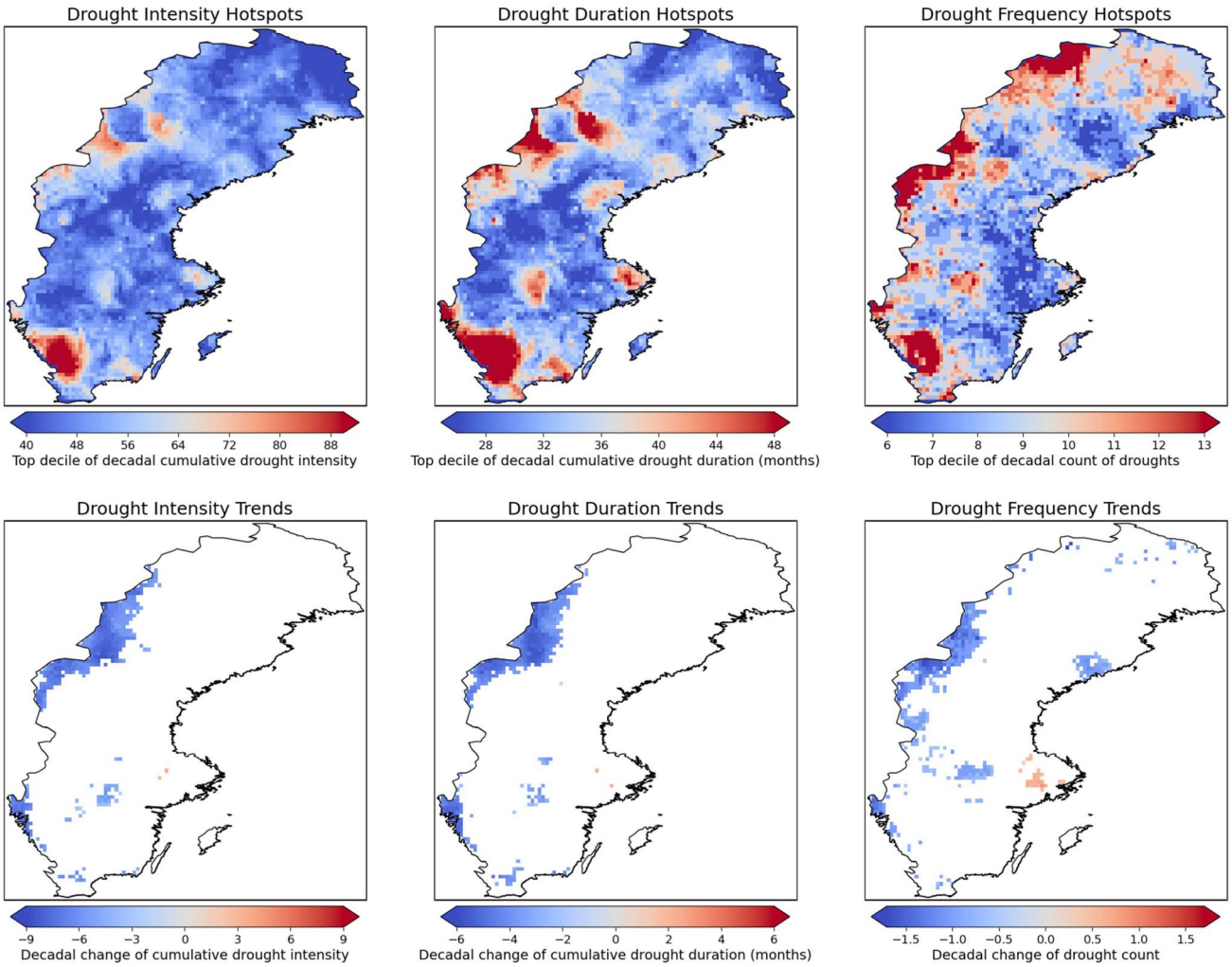

Fig. 6 Hotspots and trends in drought intensity, duration, and frequency in Sweden (Standardized Precipitation and Evapotranspiration Index, SPEI12)

during 2022–2071 can be projected if the trend continues. Increasing flood trends were observed for large areas in the southwest and north of Sweden. The trends suggest a possible extra three days per year with flood risk and one extra flood risk event per year on average after the next decade. This increasing trend is consistent with an observed increase of precipitation rates over Sweden (Teutschbein et al. 2022).

3.3 Compound hazard occurrence and dependence

Spatiotemporal patterns in compound hydroclimatic hazards were investigated by determining joint return periods of monthly hazard pairs and LMF for each hazard pair (Fig. 8, Figure S4 in SM). Three hazard pairs were considered: heatwave and drought, heatwave and flood, and drought and flood. The most frequent hazard co-occurrence observed was for droughts and heatwaves from June to August, peaking in July in southern Sweden. The LMF values indicated that heatwaves and droughts are independent in most regions during summer months, but positively correlated in the northern region, which may lead to higher compound hazard impacts there.

Co-occurrence of heatwave and flood conditions was observed only for the summer months of July and August, with very low joint exceedance probabilities. This low co-occurrence can be attributed to temperature drop effects of precipitation, e.g., due to enhanced evaporative cooling, and more cloud cover and air mass changes. Dependence analysis showed that this hazard pair was primarily characterized by a negative correlation, but LMF did not explain whether heavy rainfall is intensified if preceded by a heatwave, as it does not account for preconditioning or temporal delays between hazard events.

Compound drought and floods were more frequent in Sweden in the months from August to November (the wet season). Hotspots with lower return periods were observed

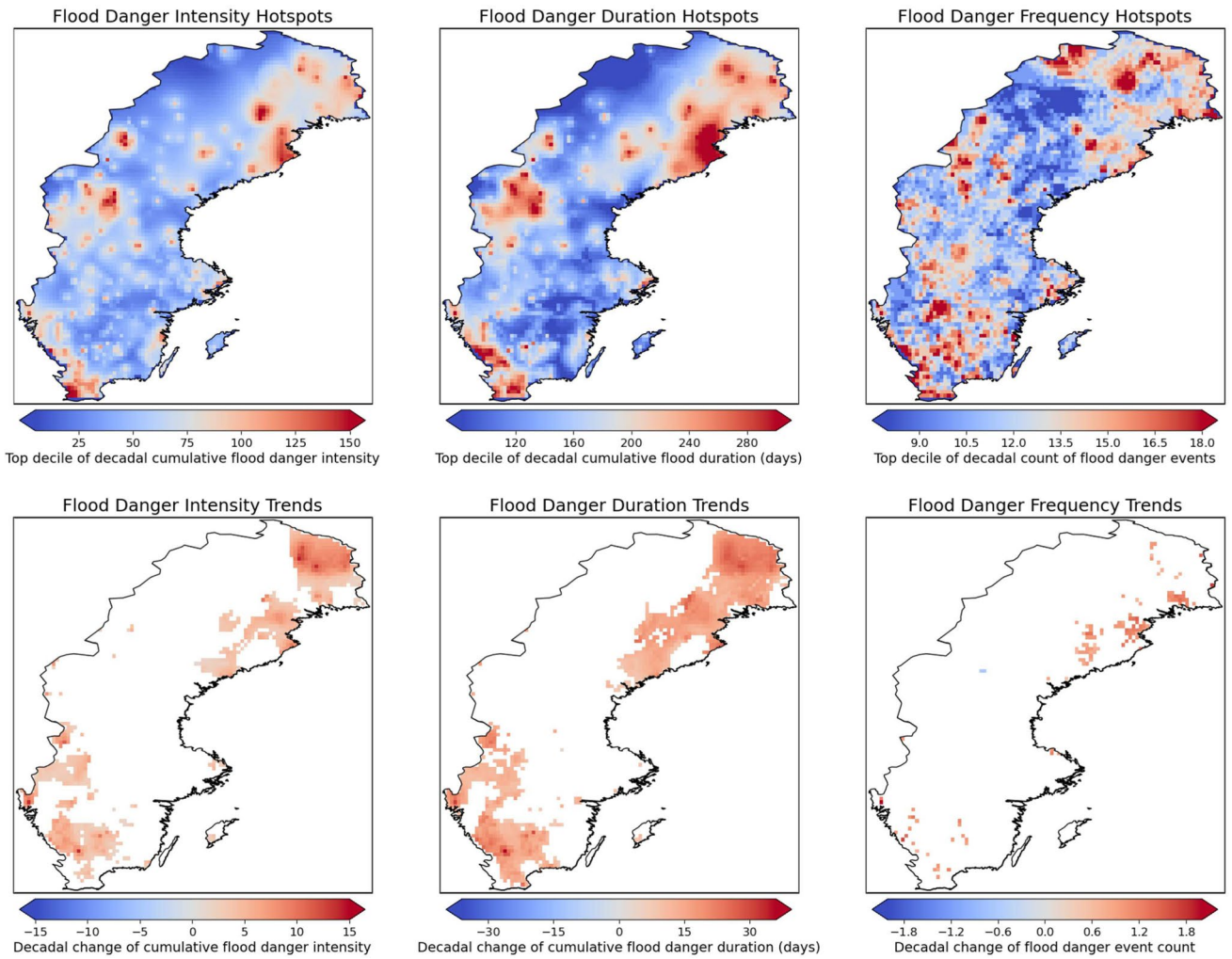

Fig. 7 Hotspots and trends in flood intensity, duration, and frequency in Sweden (Daily Flood Index, DFI)

in most southern and most northern parts of the most northern Swedish landscape, Norrland, where LMF indicated that these two hazards are positively correlated. Flood impacts in these areas can be exacerbated by increased runoff after very dry soil conditions that reduce soil permeability. In most other areas, droughts and floods are either negatively correlated or independent.

Dividing the study period into two 50-year periods (1922–1971 and 1972–2021) allowed assessment of change trends in compound hazard frequency and dependence. Figure S5 in SM shows the relative LMF change between the sub-periods for all compound hazard pairs. Heatwaves and droughts were overall the most critical hazard pair, with increasing correlation in most areas. Some areas of LMF decrease were also observed for joint heatwaves and droughts, but the magnitude of decrease was much lower than the magnitude of increase in other areas. The changes in return periods indicate that compound heatwaves and droughts are becoming more frequent in eastern Sweden, with return period decreasing by more than 100 years in some locations (Figure S6 in SM). Hotspots of increasing droughts and flood co-occurrence were observed at specific locations in the months from July to November. Some very few areas of co-occurring heatwaves and floods were found in August in both 50-year periods. The changes in LMF imply that the correlation in pairs of hazards varied spatially, but also temporally, due to various contributing factors affecting the local hazard interactions. This temporal variation indicates that it is not only individual hazards which are changing, but also their interdependencies, possibly leading to amplified consequences.

4 Discussion

Application of the framework developed in this study to the case of Sweden supported the hypothesis that the intensity, duration, and frequency of heatwaves and floods are

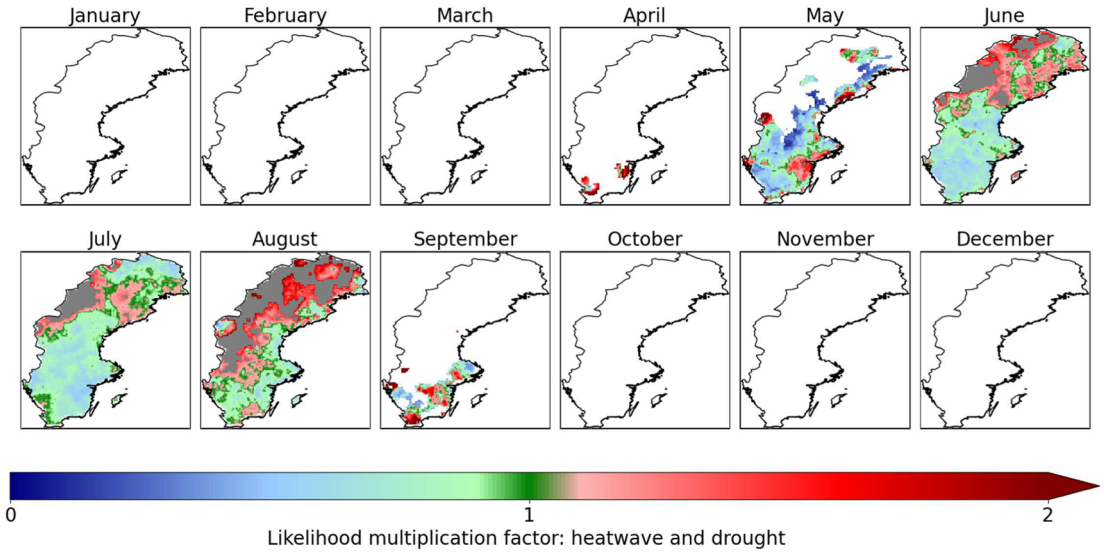
January
February
March
April
May
June
July
August
September
October
November
December
0
1
2
Likelihood multiplication factor: heatwave and drought

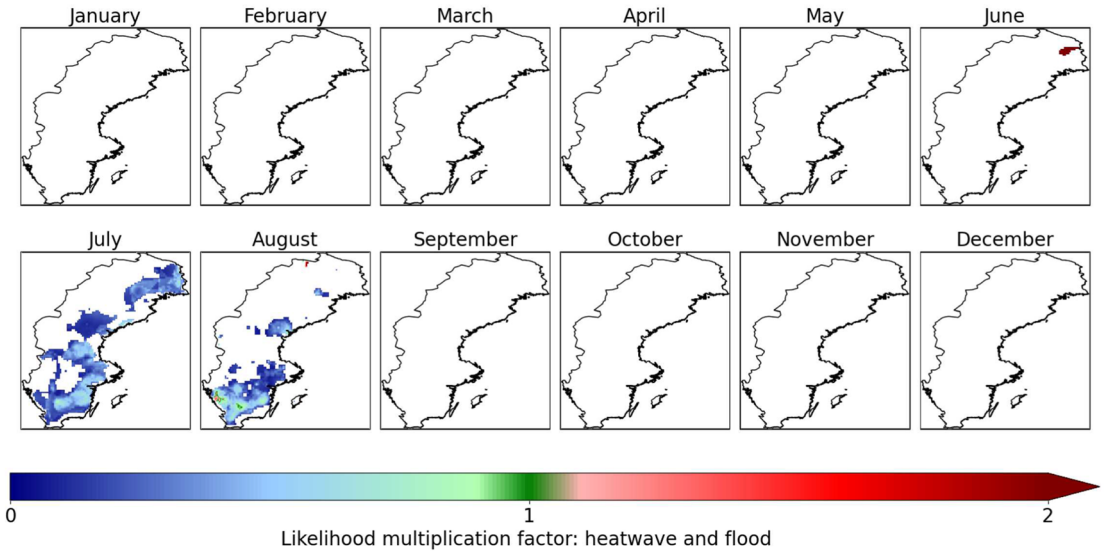
January
February
March
April
May
June
July
August
September
October
November
December
0
1
2
Likelihood multiplication factor: heatwave and flood

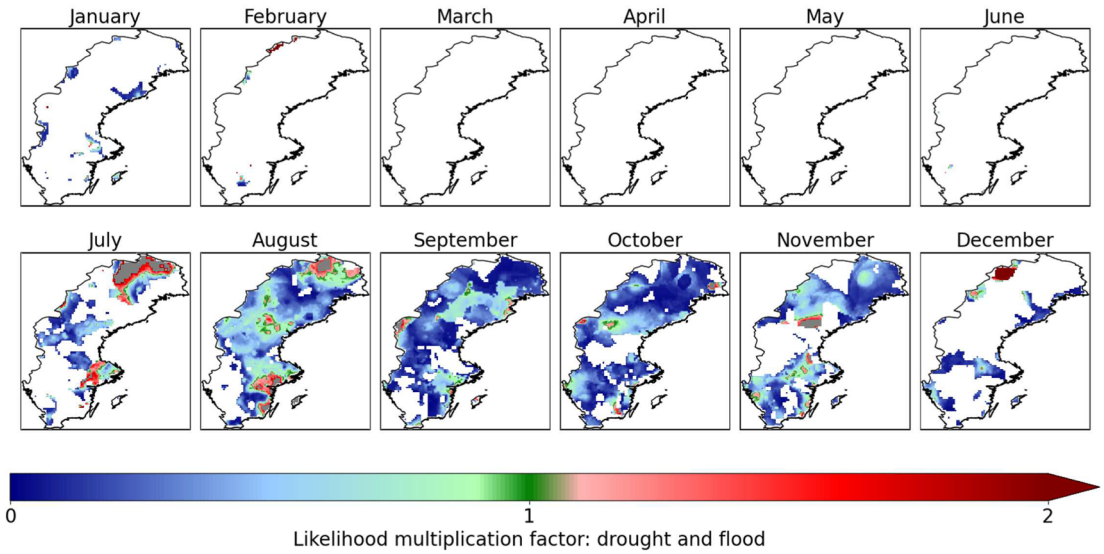
January
February
March
April
May
June
July
August
September
October
November
December
0
1
2
Likelihood multiplication factor: drought and flood

◂**Fig. 8** Distribution of likelihood multiplication factor (LMF) for different hazard pairs, based on the entire study period (1922–2021). No co-occurrences were observed in white areas. Grey areas represent grid cells where the exceedance probability was not statistically significant according to the bootstrapping method

increasing across most of the country. The most intense heatwave detected in the 100-year study period occurred in 2018 and caused significant impacts in Sweden, resulting in hundreds of excess deaths (Åström et al. 2019; Wilcke et al. 2020). However, an increasing trend was not seen for droughts. The tendency observed for wetter conditions in the country, with increasing flood risk and decreasing drought risk, is consistent with findings in a recent study on streamflow droughts in Sweden (Teutschbein et al. 2022) and in a continental integrated analysis (Lehner et al. 2006). Previous research suggests that this warming-wetting tendency with climate change may be caused by changes in the atmospheric circulation pattern (Zhang et al. 2013). The analysis of LMF and joint return periods indicated that certain regions of Sweden may experience increased impacts of co-occurrence of droughts and heatwaves, as well as droughts and floods with compound effects. Using daily frequency and a long study period provided a large sample dataset, with statistically significant observed trends and correlations.

In general, use of indices with relevant selected thresholds instead of directly measured variables for detection of extreme events has the advantage of clearly defined hazard start, end, and intensity, thereby reducing subjectivity and facilitating estimation of associated intensity, duration, and frequency trends. The ROC curve analysis proved useful for indicator validation against historical extreme events, and in selection of relevant indicators and thresholds in a regional context. Evaluation results for hazard detection performance showed similar findings as in previous studies. For example, selecting SPEI with accumulation period of 12 months as the best drought predictor is in line with conclusions from a previous drought risk assessment for Europe (Blauhut et al. 2016). The optimal SPEI threshold selected here corresponds to previously identified moderate drought conditions (Vicente-Serrano et al. 2010). Additionally, the selected DFI > 0 threshold matches a previously recommended criterion for identifying periods of flooding (Deo et al. 2015). ROC curve analysis highlighted the limitations of using monthly indicators, such as SSI, SPI, and SPEI, to detect short-term flood events, point at the need for finer temporal resolution of these indices for use in relevant flood hazard indices (Zhang et al. 2023). Overall, the statistical techniques applied to accumulate the daily precipitation values in DFI improved flood representation ability compared to the other tested flood indices outlined in Table 2. Similar techniques applied to river discharges at refined time scales (daily or hourly) could potentially further improve flood detection ability. However, testing of this improvement potential would require development of a new flood index and an associated in-depth investigation of how to formulate it based on discharge variation patterns that commonly differ greatly from the variation patterns of precipitation (e.g., Quin and Destouni (2018)), which DFI is based on. Such a new flood index investigation and formulation is not within the scope of the present comparative study of already formulated and used indices based directly on commonly available data for the whole considered study area and study period. As a main novelty, this study presents the first known application of a gridded DFI, instead of individual station data analysis. The gridding facilitates assessment of flood hazard conditions but further investigation is needed to explicitly evaluate the performance of the index at ungauged locations through cross-validation.

Assessment of individual hazards can provide good insights for regional planners, helping them prioritize areas with a higher frequency of extreme events and showing the likelihood of future hazard increases or decreases. Assessment of compound hazards can further complement these insights by offering additional information on areas that may be overlooked in individual hazard assessment, but where compound effects can exacerbate the hazard magnitude (Zscheischler et al. 2018) or create new vulnerabilities (Englund and Barquet 2023). Early warning prediction systems are also needed to decrease vulnerability and impacts of hydroclimatic hazards (Lal et al. 2012). The approach developed here can be employed in developing and evaluating such early warning systems, based on its ability to identify appropriate indicators for hazard and critical hotspot detection, indicating which hazards to prioritize. Optimal thresholds identified from actual historical occurrences of extremes are likely to represent actual high risks of impacts on infrastructure, communities, and disaster response.

This study has four major limitations. First, the number of available measurements in the first few decades of the study period is relatively low, possibly leading to inaccuracies in spatial interpolation. Even though these interpolation inaccuracies could lead to imprecise hotspots and trends, satisfactory results from the ROC method for an extensive range of years and locations show that these uncertainties are not severe. Moreover, air temperature does not vary significantly between nearby observation stations, so this limitation would mostly affect precipitation, discharge rates, and associated indices. Second, the hydroclimatic data are limited to information available up to December 2021, as the openly reported data must first go through quality checks at the agency responsible, and thus data for the most recent years of extreme events are missing. Third, soil moisture is a critical hydroclimatic variable for quantification of local-regional droughts (Orth and Destouni 2018) and their temporal trends (Destouni

and Verrot 2014) and possible predictive drought modelling (Kan et al. 2023), which was not included in this study due to lack of sufficiently long data time series. This data limitation exemplifies and highlights the challenges and uncertainties of studying long-term extreme event trends even in data-rich regions such as Sweden. Fourth, since climate indices are statistical and not process-based models, they lack detailed explanatory power to describe specific hydrometeorological processes causing the emergence of the hotspot patterns or trends.

Further research is needed to transform the hazard maps produced here into risk maps that also consider the consequences associated with the probabilities of the extreme events (Lavell et al. 2012). In this context, consequences are a function of the hazard intensity, exposure, and vulnerability. The approach developed in this study produces hazard intensities and probabilities. In order to also assess associated risks, important values and assets that can be adversely affected and their characteristics that make them susceptible to damage need to be assessed. The outputs of the approach in this study can be combined with relevant socio-economic and other impact data for hydroclimatic hazards to operationalize the concept of dynamic vulnerability (Kuran et al. 2020). Further studies are also required to investigate possible hazard preconditioning with time lags between extremes, such as possible exacerbation of floods by dry soil conditions after droughts.

Novel contributions of the methodology developed in this study include the: (1) evaluation of how well various indicators represent actual hydroclimatic hazards at local-regional level, (2) spatial distribution of patterns and trends of single hazards, and (3) mapping of co-occurring compound hazards and their characteristics and trends. The approach for mapping single and compound hydroclimatic hotspots and trends using associated high-resolution indicators is generalizable to other climate indices and types of hazards. Development of this multi-hazard approach addresses a priority for the IPCC (Lal et al. 2012) and the Sendai Framework (UNDRR-WMO 2022). To our knowledge, there are no other multi-hazard approaches for assessing hydroclimatic extremes at local-regional scale for single and compound hazard hotspots and trends of heatwaves, droughts, and flood risks. Previous studies have focused on hot-dry extremes (Laz et al. 2023; Hu et al. 2023; Wang et al. 2021), or continental-global scale (Claassen et al. 2023; Ridder et al. 2020; Zscheischler et al. 2018). The approach presented in this study is holistic, using multiple methods to assess multiple hazards starting from fundamental data collection to generation of results, supporting risk management for both single and compound effects. Transferability of the method can be hindered by lack of availability of high-quality data in other geographical areas, especially river discharge rates and catchment areas. The results obtained for Sweden exemplify one application of the framework, which can be readily adapted to different contexts and local needs by varying the input indicators.

5 Conclusions

This paper presents a novel multi-hazard approach for mapping hotspots and analyzing trends in floods, heatwaves, droughts, and their co-occurrences Using hydroclimatic indicators based on temperature, precipitation, and discharge data from thousands of observation stations over a century for the application case of Sweden, indicator performance was evaluated by direct comparison against historical extreme events at local-regional scale, to select optimal hazard indicators and thresholds. The best performing indicators for detecting hydroclimatic hazards in Sweden were found to be HWI_S, SPEI12, and DFI for heatwaves, droughts, and floods, respectively. Overall, these indicators can accurately describe the associated hazards, while monthly indices, have limited detection capability for short-term flooding events. The results revealed increasing trends for heatwave and flood hazards in Sweden, and hotspots of compound drought-heatwave and drought-flood extremes with possible exacerbated societal impacts by this hazard co-occurrence. Future research should focus on comparing hazard detection skills between local and global sources, developing models of socio-economic and other societal risks, and early warning systems for single and compound hydroclimatic hazards. Our approach and results can guide such research, predictive model and early warning developments, and practical adaptation and protection planning, by revealing critical hazard hotspots and trends, and indicating associated areas with possible high impacts.

Supplementary Information The online version contains supplementary material available at https://doi.org/10.1007/s00477-024-02783-3.

Acknowledgements We would like to thank the editor and reviewers for their constructive feedback to improve the manuscript.

Author contributions ZK, KB, and GD conceived the study. Data, software and formal analysis performed by MVP. Funding acquisition from KB, ZK, and GD. Methodology development by MVP, ZK, and JCK. Project administration by KB and ZK. Supervision from KB, ZK, and GD. All authors participated in writing the paper.

Funding Open access funding provided by Royal Institute of Technology. We are grateful for the financial support provided by the Swedish Research Council (VR) (Grant Numbers 2021-06309 and 2022-04672) and the Swedish Civil Contingencies Agency (MSB) and FORMAS (project Managing vulnerabilities to water hazards in Sweden: HydroHazards).

Data availability The framework can be reproduced using codes available on https://github.com/m-passos/hydroclimatic-hazards-hotspots

and research data available on dx.doi.org/10.6084/m9.figshare.25189118. Additional data will be made available upon reasonable request.

Declarations

Conflict of interest The authors declare that they have no known competing financial interests or personal relationships that could have appeared to influence the work reported in this paper.

References

Alfredsson C (2012) MSB: Översvämningar i Sverige 1901–2010. https://www.msb.se/sv/publikationer/oversvamningar-i-sverige-1901-2010/

Anshuka A, Van Ogtrop FF, Willem Vervoort R (2019) Drought forecasting through statistical models using standardised precipitation index: a systematic review and meta-regression analysis. Nat Hazards 97(2):955–977. https://doi.org/10.1007/s11069-019-03665-6

Åström C, Bjelkmar P, Forsberg B (2019) Attributing summer mortality to heat during 2018 heatwave in Sweden. Environ Epidemiol 3:16–17. https://doi.org/10.1097/01.EE9.0000605788.56297.b5

Avand M, Moradi HR, Ramazanzadeh Lasboyee M (2021) Spatial prediction of future flood risk: an approach to the effects of climate change. Geosciences 11(1):25. https://doi.org/10.3390/geosciences11010025

Beck HE, Zimmermann NE, McVicar TR et al (2018) Present and future Köppen–Geiger climate classification maps at 1-km resolution. Sci Data 5(1):180214. https://doi.org/10.1038/sdata.2018.214

Bergstrand M, Asp SS, Lindström G (2014) Nationwide hydrological statistics for Sweden with high resolution using the hydrological model S-HYPE. Hydrol Res 45(3):349–356. https://doi.org/10.2166/nh.2013.010

Blauhut V, Stahl K, Stagge JH et al (2016) Estimating drought risk across Europe from reported drought impacts, drought indices, and vulnerability factors. Hydrol Earth Syst Sci 20(7):2779–2800. https://doi.org/10.5194/hess-20-2779-2016

Bradley AP (1997) The use of the area under the ROC curve in the evaluation of machine learning algorithms. Pattern Recogn 30(7):1145–1159. https://doi.org/10.1016/S0031-3203(96)00142-2

Byun HR, Lee DK (2002) Defining three rainy seasons and the hydrological summer Monsoon in Korea using available water resources index. J Meteorol Soc Jpn Ser II 80(1):33–44. https://doi.org/10.2151/jmsj.80.33

Claassen JN, Ward PJ, Daniell J et al (2023) A new method to compile global multi-hazard event sets. Sci Rep 13(1):13808. https://doi.org/10.1038/s41598-023-40400-5

Coscarelli R, Aguilar E, Petrucci O et al (2021) The potential role of climate indices to explain floods, mass-movement events and wildfires in Southern Italy. Climate 9(11):156. https://doi.org/10.3390/cli9110156

Darand M, Sohrabi MM (2018) Identifying drought- and flood-prone areas based on significant changes in daily precipitation over Iran. Nat Hazards 90(3):1427–1446. https://doi.org/10.1007/s11069-017-3107-9

Deo RC, Byun HR, Adamowski JF et al (2015) A real-time flood monitoring index based on daily effective precipitation and its application to Brisbane and Lockyer valley flood events. Water Resour Manag 29(11):4075–4093. https://doi.org/10.1007/s11269-015-1046-3

Deo RC, Adamowski JF, Begum K et al (2019) Quantifying flood events in Bangladesh with a daily-step flood monitoring index based on the concept of daily effective precipitation. Theoret Appl Climatol 137(1–2):1201–1215. https://doi.org/10.1007/s00704-018-2657-4

Destouni G, Verrot L (2014) Screening long-term variability and change of soil moisture in a changing climate. J Hydrol 516:131–139. https://doi.org/10.1016/j.jhydrol.2014.01.059

Dikshit A, Pradhan B, Huete A (2021) An improved SPEI drought forecasting approach using the long short-term memory neural network. J Environ Manag 283:111979. https://doi.org/10.1016/j.jenvman.2021.111979

Englund M, Barquet K (2023) Threatification, riskification, or normal politics? A review of Swedish climate adaptation policy 2005–2022. Clim Risk Manag 40:100492. https://doi.org/10.1016/j.crm.2023.100492

Freire-González J, Decker C, Hall JW (2017) The economic impacts of droughts: a framework for analysis. Ecol Econ 132:196–204. https://doi.org/10.1016/j.ecolecon.2016.11.005

Guerreiro SB, Dawson RJ, Kilsby C et al (2018) Future heat-waves, droughts and floods in 571 European cities. Environ Res Lett 13(3):034009. https://doi.org/10.1088/1748-9326/aaaad3

Guvenir HA, Kurtcephe M (2013) Ranking instances by maximizing the area under ROC curve. IEEE Trans Knowl Data Eng 25(10):2356–2366. https://doi.org/10.1109/TKDE.2012.214

Hargreaves GH, Samani ZA (1985) Reference crop evapotranspiration from temperature. Appl Eng Agric 1(2):96–99. https://doi.org/10.13031/2013.26773

He RR, Chen Y, Huang Q et al (2018) Evaluation of ocean-atmospheric indices as predictors for summer streamflow of the Yangtze River based on ROC analysis. Stoch Env Res Risk Assess 32(7):1903–1918. https://doi.org/10.1007/s00477-018-1551-z

He Q, Wang M, Liu K et al (2022) GPRChinaTemp1km: A high-resolution monthly air temperature data set for China (1951–2020) based on machine learning. Earth Syst Sci Data 14(7):3273–3292. https://doi.org/10.5194/essd-14-3273-2022

Hu Z, Hu Q, Zhang C et al (2016) Evaluation of reanalysis, spatially interpolated and satellite remotely sensed precipitation data sets in central Asia. J Geophys Res Atmos 121(10):5648–5663. https://doi.org/10.1002/2016JD024781

Hu J, Yang Z, Hou C et al (2023) Compound risk dynamics of drought by extreme precipitation and temperature events in a semi-arid watershed. Atmos Res 281:106474. https://doi.org/10.1016/j.atmosres.2022.106474

Intergovernmental Panel on Climate Change (IPCC) (2023) Climate change 2022—Impacts, Adaptation and Vulnerability: Working Group II Contribution to the Sixth Assessment Report of the Intergovernmental Panel on Climate Change, 1st edn. Cambridge University Press, Cambridge. https://doi.org/10.1017/9781009325844

Kan JC, Ferreira CS, Destouni G et al (2023) Predicting agricultural drought indicators: ML approaches across wide-ranging climate and land use conditions. Ecol Ind 154:110524. https://doi.org/10.1016/j.ecolind.2023.110524

Kappes MS, Keiler M, Von Elverfeldt K et al (2012) Challenges of analyzing multi-hazard risk: a review. Nat Hazards 64(2):1925–1958. https://doi.org/10.1007/s11069-012-0294-2

Kirono DG, Round V, Heady C et al (2020) Drought projections for Australia: updated results and analysis of model simulations. Weather Clim Extremes 30:100280. https://doi.org/10.1016/j.wace.2020.100280

Kleiber W, Katz RW, Rajagopalan B (2012) Daily spatiotemporal precipitation simulation using latent and transformed Gaussian processes. Water Resources Res 48(1):2011WR011105. https://doi.org/10.1029/2011WR011105

Kumar R, Musuuza JL, Van Loon AF et al (2016) Multiscale evaluation of the Standardized Precipitation Index as a groundwater drought indicator. Hydrol Earth Syst Sci 20(3):1117–1131. https://doi.org/10.5194/hess-20-1117-2016

Kundzewicz Z, Krysanova V, Benestad R et al (2018) Uncertainty in climate change impacts on water resources. Environ Sci Policy 79:1–8. https://doi.org/10.1016/j.envsci.2017.10.008

Kuran CHA, Morsut C, Kruke BI et al (2020) Vulnerability and vulnerable groups from an intersectionality perspective. Int J Disaster Risk Reduct 50:101826. https://doi.org/10.1016/j.ijdrr.2020.101826

Lal PN, Mitchell T, Aldunce P, et al (2012) National systems for managing the risks from climate extremes and disasters. In: Field CB, Barros V, Stocker TF et al (eds) Managing the risks of extreme events and disasters to advance climate change adaptation, 1st edn. Cambridge University Press, Cambridge, pp 339–392. https://doi.org/10.1017/CBO9781139177245.009

Lavaysse C, Cammalleri C, Dosio A et al (2018) Towards a monitoring system of temperature extremes in Europe. Nat Hazard 18(1):91–104. https://doi.org/10.5194/nhess-18-91-2018

Lavell A, Oppenheimer M, Diop C, et al (2012) Climate change: new dimensions in disaster risk, exposure, vulnerability, and resilience. In: Field CB, Barros V, Stocker TF et al (eds) Managing the risks of extreme events and disasters to advance climate change adaptation. Cambridge University Press, Cambridge, pp 25–64. https://doi.org/10.1017/CBO9781139177245.004

Laz OU, Rahman A, Ouarda TBMJ (2023) Compound heatwave and drought hotspots and their trends in Southeast Australia. Nat Hazards 119(1):357–386. https://doi.org/10.1007/s11069-023-06115-6

Lehner B, Döll P, Alcamo J et al (2006) Estimating the impact of global change on flood and drought risks in Europe: a continental, integrated analysis. Clim Change 75(3):273–299. https://doi.org/10.1007/s10584-006-6338-4

Lian X, Huang J, Li H et al (2023) Heat waves accelerate the spread of infectious diseases. Environ Res 231:116090. https://doi.org/10.1016/j.envres.2023.116090

Lindström G, Pers C, Rosberg J et al (2010) Development and testing of the HYPE (Hydrological Predictions for the Environment) water quality model for different spatial scales. Hydrol Res 41(3–4):295–319. https://doi.org/10.2166/nh.2010.007

Lloyd-Hughes B, Saunders MA (2002) A drought climatology for Europe. Int J Climatol 22(13):1571–1592. https://doi.org/10.1002/joc.846

López-Bueno JA, Díaz J, Follos F et al (2021) Evolution of the threshold temperature definition of a heat wave vs. evolution of the minimum mortality temperature: a case study in Spain during the 1983–2018 period. Environ Sci Eur. https://doi.org/10.1186/s12302-021-00542-7

Modarres R (2007) Streamflow drought time series forecasting. Stoch Environ Res Risk Assess 21(3):223–233. https://doi.org/10.1007/s00477-006-0058-1

Moishin M, Deo RC, Prasad R et al (2021) Development of Flood Monitoring Index for daily flood risk evaluation: case studies in Fiji. Stoch Environ Res Risk Assess 35(7):1387–1402. https://doi.org/10.1007/s00477-020-01899-6

Nkiaka E, Nawaz NR, Lovett JC (2017) Using standardized indicators to analyse dry/wet conditions and their application for monitoring drought/floods: a study in the Logone catchment, Lake Chad basin. Hydrol Sci J 62(16):2720–2736. https://doi.org/10.1080/02626667.2017.1409427

Orth R, Destouni G (2018) Drought reduces blue-water fluxes more strongly than green-water fluxes in Europe. Nat Commun 9(1):3602. https://doi.org/10.1038/s41467-018-06013-7

Quin A, Destouni G (2018) Large-scale comparison of flow-variability dampening by lakes and wetlands in the landscape. Land Degrad Dev 29(10):3617–3627. https://doi.org/10.1002/ldr.3101

Rahmati O, Yousefi S, Kalantari Z et al (2019) Multi-hazard exposure mapping using machine learning techniques: a case study from Iran. Remote Sens 11(16):1943. https://doi.org/10.3390/rs11161943

Rasmussen CE, Williams CKI (2005) Gaussian processes for machine learning. The MIT Press, Cambridge. https://doi.org/10.7551/mitpress/3206.001.0001

Ridder NN, Pitman AJ, Westra S et al (2020) Global hotspots for the occurrence of compound events. Nat Commun 11(1):5956. https://doi.org/10.1038/s41467-020-19639-3

Salimi H, Asadi E, Darbandi S (2021) Meteorological and hydrological drought monitoring using several drought indices. Appl Water Sci 11(2):11. https://doi.org/10.1007/s13201-020-01345-6

Serrano-Notivoli R, Lemus-Canovas M, Barrao S et al (2022) Heat and cold waves in mainland Spain: origins, characteristics, and trends. Weather Clim Extremes 37:100471. https://doi.org/10.1016/j.wace.2022.100471

Shin JY, Kwon HH, Lee JH et al (2020) Probabilistic long-term hydrological drought forecast using Bayesian networks and drought propagation. Meteorol Appl 27(1):e1827. https://doi.org/10.1002/met.1827

Šípek V, Daňhelka J (2015) Modification of input datasets for the Ensemble Streamflow Prediction based on large-scale climatic indices and weather generator. J Hydrol 528:720–733. https://doi.org/10.1016/j.jhydrol.2015.07.008

SMHI (2011) Värmeböljor i Sverige | SMHI. https://www.smhi.se/polopoly_fs/1.16889!/webbFaktablad_49.pdf

SMHI (2019) 1947 - Lite snö och torr sommar | SMHI. https://www.smhi.se/kunskapsbanken/hydrologi/historiska-torrperioder/torrar-1947-1.151109?l=null

SMHI (2023a) Historiska torrperioder | SMHI. https://www.smhi.se/kunskapsbanken/hydrologi/historiska-torrperioder/historiska-torrperioder-1.151112

SMHI (2023b) SMHI Open Data API Documentation. https://opendata.smhi.se/apidocs/

SMHI (2024a) Databaser och kartmaterial | SMHI. https://www.smhi.se/data/hydrologi/svenskt-vattenarkiv

SMHI (2024b) Vattenwebb smhi. https://www.smhi.se/data/hydrologi/vattenwebb

Stagliorio Coelho MDSZ, Matera Veras M, Nascimento Saldiva PH (2023) The biologic mechanism for heat exposure and human health. In: Heat exposure and human health in the context of climate change. Elsevier, New York, pp 37–67. https://doi.org/10.1016/B978-0-12-819080-7.00001-X

Stenseth NC, Ottersen G, Hurrell JW et al (2003) Studying climate effects on ecology through the use of climate indices: the North Atlantic Oscillation, El Niño Southern Oscillation and beyond. Proc R Soc Lond B 270(1529):2087–2096. https://doi.org/10.1098/rspb.2003.2415

Stevenson S, Coats S, Touma D et al (2022) Twenty-first century hydroclimate: a continually changing baseline, with more frequent

extremes. Proc Natl Acad Sci 119(12):e2108124119. https://doi.org/10.1073/pnas.2108124119
Stone DA (2019) A hierarchical collection of political/economic regions for analysis of climate extremes. Clim Change 155(4):639–656. https://doi.org/10.1007/s10584-019-02479-6
Suursaar Ü (2020) Combined impact of summer heat waves and coastal upwelling in the Baltic Sea. Oceanologia 62(4):511–524. https://doi.org/10.1016/j.oceano.2020.08.003
Teutschbein C (2024) Camels-se: Long-term hydroclimatic observations (1961–2020) across 50 catchments in Sweden as a resource for modelling, education, and collaboration. Geosci Data J. https://doi.org/10.1002/gdj3.239
Teutschbein C, Quesada Montano B, Todorović A et al (2022) Streamflow droughts in Sweden: spatiotemporal patterns emerging from six decades of observations. J Hydrol Reg Stud 42:101171. https://doi.org/10.1016/j.ejrh.2022.101171
Thompson V, Mitchell D, Hegerl GC et al (2023) The most at-risk regions in the world for high-impact heatwaves. Nat Commun 14(1):2152. https://doi.org/10.1038/s41467-023-37554-1
UNCED (1993) Agenda 21: programme of action for sustainable development, Rio declaration on environment and development, statement of forest principles: the final text of agreements negotiated by governments at the united nations conference on environment and development (UNCED), 3–14 June 1992, Rio de Janeiro, Brazil. http://digitallibrary.un.org/record/170126, on cover: Earth Summit, Agenda 21, the United Nations programme of action from Rio
UNDRR-WMO (2022) Global status of multi-hazard early warning systems 2022 | UNDRR. https://www.undrr.org/publication/global-status-multi-hazard-early-warning-systems-2022
Vicente-Serrano SM, Beguería S, López-Moreno JI (2010) A multiscalar drought index sensitive to global warming: the standardized precipitation evapotranspiration index. J Clim 23(7):1696–1718. https://doi.org/10.1175/2009JCLI2909.1
Wang W, Zhang Y, Guo B et al (2021) Compound droughts and heatwaves over the Huai River Basin of China: from a perspective of the magnitude index. J Hydrometeorol. https://doi.org/10.1175/JHM-D-20-0305.1
Wilcke RAI, Kjellström E, Lin C et al (2020) The extremely warm summer of 2018 in Sweden—set in a historical context. Earth Syst Dyn 11(4):1107–1121. https://doi.org/10.5194/esd-11-1107-2020
Xiao J, Spicer T, Jian L et al (2017) Variation in population vulnerability to heat wave in western Australia. Front Public Health 5:64. https://doi.org/10.3389/fpubh.2017.00064
Xue JH, Hall P (2015) Why does rebalancing class-unbalanced data improve AUC for linear discriminant analysis? IEEE Trans Pattern Anal Mach Intell 37(5):1109–1112. https://doi.org/10.1109/TPAMI.2014.2359660
Yang P, Xia J, Luo X et al (2021) Impacts of climate change-related flood events in the Yangtze River Basin based on multi-source data. Atmos Res 263:105819. https://doi.org/10.1016/j.atmosres.2021.105819
Zhang X, He J, Zhang J et al (2013) Enhanced poleward moisture transport and amplified northern high-latitude wetting trend. Nat Clim Change 3(1):47–51. https://doi.org/10.1038/nclimate1631
Zhang R, Bento VA, Qi J et al (2023) The first high spatial resolution multi-scale daily SPI and SPEI raster dataset for drought monitoring and evaluating over China from 1979 to 2018. Big Earth Data 7(3):860–885. https://doi.org/10.1080/20964471.2022.2148331
Zscheischler J, Seneviratne SI (2017) Dependence of drivers affects risks associated with compound events. Sci Adv 3(6):e1700263. https://doi.org/10.1126/sciadv.1700263
Zscheischler J, Westra S, Van Den Hurk BJJM et al (2018) Future climate risk from compound events. Nat Clim Change 8(6):469–477. https://doi.org/10.1038/s41558-018-0156-3
Zscheischler J, Martius O, Westra S et al (2020) A typology of compound weather and climate events. Nat Rev Earth Environ 1(7):333–347. https://doi.org/10.1038/s43017-020-0060-z